Supra-molecular assemblies of ORAI1 at rest precede local accumulation into punctae after activation

Diana B. Peckys[1], Dalia Alansary[1], Barbara. A. Niemeyer[1] and Niels de Jonge[2, 3*]

[1]Molecular Biophysics, University of Saarland, Center for Integrative Physiology and Molecular Medicine, 66421 Homburg/Saar, Germany

[2]INM – Leibniz Institute for New Materials, 66123 Saarbrücken, Germany

[3]Department of Physics, University of Saarland, 66123 Saarbrücken, Germany

[*]To whom correspondence may be addressed: niels.dejonge@leibniz-inm.de

Running title: supra-molecular ORAI1 assemblies

ABSTRACT

The Ca^{2+} selective channel ORAI1 and endoplasmic reticulum (ER)-resident STIM proteins form the core of the channel complex mediating store operated Ca^{2+} entry (SOCE). Using liquid phase electron microscopy (LPEM) the distribution of ORAI1 proteins was examined at rest and after SOCE-activation at nanoscale resolution. The analysis of over seven hundred thousand of ORAI1 positions showed that already at rest, a majority of the ORAI1 channels formed STIM-independent distinct supra-molecular clusters. Upon SOCE activation and in the presence of STIM proteins, ORAI1 assembled in micron-sized two-dimensional (2D) structures, such as the known punctae at the ER plasma membrane contact zones, but also in divergent structures such as strands, and ring-like shapes. Our results thus question the hypothesis that stochastically migrating single ORAI1 channels are trapped at regions containing activated STIM, and we propose instead that supra-molecular ORAI1 clusters fulfill an amplifying function for creating dense ORAI1 accumulations upon SOCE-activation.

STATEMENT OF SIGNIFICANCE

ORAI1 proteins form channels mediating store operated Ca^{2+} entry, an important trigger for many cellular functions, especially in the immune system. ORAI1 channels at rest are assumed to be randomly distributed in the plasma membrane, while they accumulate into so-called “punctae” upon activation, where binding by STIM proteins activate the Ca^{2+} channels. Using liquid phase electron microscopy, we discovered that ORAI1 forms small, elongated and linear clusters indicating the existence of supramolecular assemblies. The role of such supramolecular organization of ORAI1 is possibly an amplifying function for the effective creation of ORAI1 accumulations in punctae, since the binding of only one ORAI1 protein would trap a multiple of channels.

INTRODUCTION

The molecular processes preceding and optimizing the activation of store-operated calcium entry (SOCE) are difficult to study because they require single molecule resolution, while at the same time, the interaction of a multiple of proteins needs to be examined (1, 2). After several early reports supported tetrameric ORAI1 conformations (3-6) the current view is that ORAI1 proteins assemble as a hexameric channel complex at rest (7, 8), and that these hexameric protein complexes are randomly distributed throughout the plasma membrane. Upon Ca^{2+} store depletion, STIM proteins redistribute in the endoplasmic reticulum (ER) membrane towards the cytosolic side of ER plasma membrane contact zones, where typical, dense STIM1 accumulations, so-called punctae are formed (9, 10). In these junctional areas between ER and plasma membrane, STIM1 proteins approach the plasma membrane on the cytoplasmic side where they interact with ORAI1, resulting in a conformational change that opens the ORAI1 channels. Yet, how the ORAI1 channels translocate to these regions in order to get trapped there is not fully understood. It is assumed that single ORAI1 channels randomly diffuse by Brownian motion within the plasma membrane, until they arrive at sites of activated STIM1, so-called punctae (2). Here, ORAI1 binds to STIM1, leading to an accumulation of ORAI1 in the plasma membrane, above the STIM punctae, thus mirroring the distribution pattern of the punctae but then at the cell exterior, accompanied by activation of the Ca^{2+} channels, resulting in a local Ca^{2+} influx (2). But possibly different mechanisms play a role, for example, the additional insertion of ORAI1 from intracellular stores into the regions of punctae (11), or potentially a pre-clustering of several hexamers which are then pulled into the ER-PM junctions.

By using liquid phase electron microscopy (LPEM) capable of studying ORAI1 proteins in the plasma membrane of intact cells (12, 13), we set out to examine the difference in spatial distribution of ORAI1 between cells at rest and upon SOCE-activation. Our aim was

to test 1) if single ORAI1 channels are indeed randomly distributed at rest, and then move into clusters as independent entities, and 2) if activated clusters show distinct patterns. For this purpose, ORAI1 proteins with a stoichiometric expression of cytosolic GFP and with a human influenza (HA) tag located in the extracellular loop between transmembrane regions (TM) 3 and 4, were expressed in HEK cells, and labeled with quantum dots providing both a fluorescence label for light microscopy, and a nanoparticle label for detection with electron microscopy (12, 13). Fig. 1a depicts the dimensions of an ORAI1 hexamer (7) in a hypothetical arrangement of three QD labels bound to the same ORAI1 hexamer. Due to the flexibility of the linker, the center-to-center distance between both QDs may vary between 20 and 40 nm. Spatial patterns of individual QD labels on whole cells were imaged under resting conditions, and after two methods of SOCE-activation. The spatial distributions of the labeled ORAI1 proteins were subsequently analyzed with nanometer spatial resolution.

MATERIALS AND METHODS

Materials

Fetal bovine serum, 2-mercaptoethanol (ME), thapsigargin (Tg), cyclopiazonic acid (CPA), and sodium azide, were either from Fisher Scientific or Sigma Aldrich. ScreenFect®A Transfection reagent was from Incella GmbH, Eggenstein-Leopoldshafen, Germany. Anti-HA-biotin, high affinity (3F10) from rat IgG1 was from Roche Diagnostics, Mannheim, Germany. Dulbecco's phosphate buffered saline (DPBS), Modified Eagle's Medium (MEM), normal goat serum (GS), CellStripper and quantum dot Qdot® 655 streptavidin conjugates (QD) were from Fisher Scientific GmbH, Schwerte, Germany. ROTISOLV® high pressure liquid chromatography grade pure water, acetone and ethanol, phosphate buffered saline (PBS) 10 × solution, electron microscopy grade glutaraldehyde (GA) 25% solution, D-saccharose, sodium chloride, glycine, biotin free and molecular biology grade albumin

fraktion V (BSA), and sodium cacodylate trihydrate were from Carl Roth GmbH + Co. KG, Karlsruhe, Germany. Electron microscopy grade formaldehyde (FA) 16% solution was from Science Services GmbH, Munich, Germany. 0.01% poly-L-Lysine (PLL) solution (mol wt. 70,000-150,000), sodium tetraborate, and boric acid were from Sigma-Aldrich Chemie GmbH, Munich, Germany. CELLVIEW cell culture dishes (35 mm) with four compartments and glass bottoms were from Greiner Bio-One GmbH, 72636 Frickenhausen. Custom designed silicon microchips were purchased from DENSsolution, Netherlands. The microchips had outer dimensions of $2.0 \times 2.6 \times 0.4$ mm^3 and each contained a silicon nitride (SiN) membrane window, usually with dimensions of 150×400 µm^2 (sometimes larger) along with a membrane of 50 nm thickness. Trivial transfer multilayer graphene was purchased from ACS Material LLC, Pasadena, CA, USA. $NaCl_2$ crystals were from Plano GmbH, Wetzlar, Germany.

HEK293 cells were obtained from ATCC and genetically modified using CRISPR/Cas9-mediated gene deletion of endogenous ORAI1-2 genes (named HEK CRI1), or ORAI1-3 genes (named HEK_CRI2, which were used for controls shown in the Fig. S2), as described in (12). A HEK cells line lacking endogenous STIM proteins (HEK_STIM) (14) was obtained from was obtained from Donald L. Gill (14). An ORAI1 construct with an extracellular, nine amino acid HA-tag within the second extracellular loop of ORAI1, was used for labeling the protein with a QD (15). The DNA construct contained also DNA encoding green fluorescent protein (GFP) but separated by a cleavable peptide sequence (P2A) thus guaranteeing the same expression ratio (13, 16).The ORAI1-GFP DNA construct was transiently expressed in the HEK cells using ScreenFect®A as described in (12).

Preparation of microchips with transfected HEK cells

CELLVIEW dishes and microchips with thin SiN windows were used as a support for HEK CRI1 cells. Preparation of new microchips was performed as described previously (17),

briefly, protective photoresist coating on the microchips was removed with acetone and ethanol, the microchips and dishes were plasma-cleaned for 5 minutes, coated with PLL, and immersed/filled with cell medium (supplemented with 10% FBS and 50 μM ME). Cells grown in a 25 cm^2 flask were harvested at ~90% confluency, and washed once in supplemented cell medium. Cell transfection was performed according the supplier instructions. In experiments with ORAI1 at rest, 0.25 μg ORAI1-HA DNA and 1.5 μL transfection reagent (TR) were used per compartment of a 4-compartment dish (35 mm diameter) containing a final volume of 420 μL cell suspension. In experiments with activated ORAI1, 0.17 μg ORAI1-HA DNA, 0.55 μg STIM1-mcherry DNA, to yield a 1:3 ratio between ORAI1 and STIM1, or 0.17 μg for each DNA and 2 μL TR, for a 1:1 ratio, were used per dish compartment. The respective volumes for single microchips kept in wells of a 96-well plate were 25% of those used for dish compartments. The cell samples were then incubated for 24 hours in the CO_2 incubator.

Labeling of overexpressed ORAI1-HA at rest or after activation

A two-step labeling protocol (13, 17) was applied using a biotinylated anti-HA Fab, followed by labeling with QD, as previously described (12). After transfection, the samples were rinsed with supplemented cell medium pre-warmed to 37°C. For experiments examining unstimulated ORAI1 distribution, the samples were rinsed in pre-warmed 0.1 M cacodyl buffer containing 0.1 M sucrose, pH 7.4 (CB), and incubated in 3% formaldehyde/0.2% glutaraldehyde in CB for 10 minutes at room temperature, thereby assuring fast and strong immobilization of membrane proteins (18, 19). For the examination of activated ORAI, cells were first rinsed twice with pre-warmed medium (MEM, suppl. with 10% FCS and 50 μM ME), then incubated with 1 μM Tg, or 30 μM CPA (both in supplemented medium), for 15 min at 37 °C (in the CO2 incubator). The activated cells were rinsed once with pre-warmed medium, and once with pre-warmed CB, followed by fixation as described above. Fixation

was terminated by rinsing once with CB, three times with PBS, 2 min of incubation in GLY-PBS (0.1% glycine in PBS) for 2 minutes, followed by a rinse in PBS. The cells were then incubated in 400 ng/mL Anti-HA-Fab-Biotin lab. sol. in PBS, first for 1 hour at room temperature, followed by 3 – 6 hours at 4°C. The QD-labeling solutions were prepared by first diluting 1 µM Streptavidin-QD stock solutions 1: 5 in 40 mM Borate buffer, pH 8.3, and a further dilution in hBSA-PBS (PBS with 1% BSA) to obtain a 20 nM QD labeling solution. After three times rinsing in PBS, cells were incubated in the streptavidin-QD labeling solutions for 12 minutes at room temperature. Since no unspecific binding occurred without addition of BSA, it was omitted in the processing steps before the QD-incubation. After the QD incubation, the cells were rinsed four times with hBSA-PBS before fluorescence microscopy was performed.

Fluorescence Microscopy

After QD incubation and before the second fixation step, cells on microchips were imaged with an inverted fluorescence microscope (DMI6000B Leica, Germany) in a pristine, 35 mm cell culture glass-bottom dish filled with 2 mL hBSA-PBS. 20x and 40x objectives were used together with filter cubes for direct interference contrast (DIC), or fluorescence filters specific for QD (filter cube A) absorption and emission wavelengths. The imaging settings for each fluorescence signal were kept identical between different samples to allow for quantification.

Processing of samples for LPEM

To stabilize the cells on the microchips for electron microscopy, the aforementioned samples were further fixed with 2% glutaraldehyde in CB for 10 minutes at room temperature. After one rinse with CB, and three rinses with hBSA-PBS, they were stored in hBSA-PBS supplemented with 0.02% sodium azide, at 4°C until liquid-phase STEM, usually performed within 1- 3 weeks. To keep the ORAI channels in their almost native environment, as provided by the imaging of hydrated, intact cells, the microchip samples were covered with

graphene. Multi-layer (3 to 5 layers) graphene on polymer was cleaned and transferred onto the sample as described previously (20, 21). For the coating of a microchip sample, a graphene sheet of approximately the size of a microchip was detached from its supporting NaCl crystal through immersion in a beaker filled with HPLC-grade water, placed under a binocular. The (wet) microchip was grabbed with a pair of fine-tipped tweezers, rinsed twice with pure water, and immersed in the liquid below the floating graphene. The graphene was then carefully scooped up by slowly drawing the microchip up and out of the water. The tweezers tips, still holding the microchip with the on top swimming graphene sheet, were fixed with a small rubber O-ring, and the other tweezer end was clamped into a small stand, so that the microchip hang free in the air. After a few minutes dry time the water on the graphene had evaporated and the graphene was directly adhering to the underlying, still hydrated cells, a detailed description of this step can be found elsewhere (20).

LPEM of QD-labeled whole cells

To observe the individual QD-labeled ORAI1-HA positions, the graphene-coated samples were imaged in a transmission electron microscope (ARM 200, JEOL, Japan), with STEM dark field mode (20). The following settings were used: electron energy of 200 kV, and 175 pA probe current. For orientation purpose, the imaging session started with the recording of two to three overview STEM images, covering the entire SiN-window area. These low magnification images were directly compared to the previously recorded fluorescence- and DIC images and served to navigate to selected, representative cells chosen for high-magnification imaging. Several images from selected QD-labeled cells were recorded from randomly chosen plasma membrane regions. Note that central areas in the thickest, nucleus containing part of the cells were excluded. Images were recorded with magnifications of mostly 60.000× (occasionally, other magnifications ranging between 40,000 and 100,000× were applied), resulting in a pixel size of 1.7 nm. The image size of the 16-bit images was

2048 × 2048 pixels, comprising a scanning area of 11.7 µm² per 60.000× magnified image. The used pixel dwell-times ranged between 10 and 14 µs. The calculated electron doses was maximal 53 $e^-/Å^2$, much lower than the known limit of radiation damage for these samples (22).

Particle detection

In order to obtain the lateral coordinates of the QD labels, all STEM images were first visually screened for infrequently occurring contaminants on the graphene (remnants of the production process) with dimensions and contrast characteristics sometimes hampering the automated label detection. In such cases, ImageJ (version 1.52a, NIH) was used to manually blank the respective contaminant in the image by covering them with a fitting shape, filled with the grey value of the surrounding background. QD labels were detected and localized by applying a dedicated Plugin of local design in ImageJ described elsewhere (23). The main processing steps consisted of a Fourier filter for spatial frequencies between a factor of 3 smaller and a factor of 3 higher than the set size (8 nm), and a binarization with an automated threshold with a maximum entropy setting. The particles were automatically detected using the "Find Particles" tool, with a precision corresponding to the pixel size of 1.6 nm.

For a better visual perception of the arrangement of labeled ORAI in selected images, we implemented another PlugIn of local design. This was related to the fact that only the core of the QDs created sufficient STEM contrast, but not the shell, the polymer layer and the conjugated streptavidin. QD655 exhibited a bullet-shaped core of dimensions of 7 x 12 nm^2, and the thickness of the surrounding layer amounted to ~6 nm (12). Improved visual pattern recognition of the arranged labels was achieved by using the x-y center position data form the detected labels in a STEM image, and drawing black circles with the actual total diameter of the detected QD type, on a blank image background of the same dimensions as the STEM image.

The x-y center position data form the detected labels in all analyzed images were further analyzed statistically with the $g(r)$ function, which yields the probability of finding the center of a particle at a given distance from the center of any other particle. The pair correlation function can return information if the particles are distributed by chance or if preferred particle distances occurred with frequencies deviating from randomness.

Analysis of supra-molecular ORAI1 arrangements and punctae

For the analysis of linear ORAI1 arrangements, 6 representative STEM images from 5 cells under resting conditions, and 7 images from 6 cells after maximal SOCE-activation, were visually inspected, and all detectable label chains consisting of at least 4 linearly aligned labels were analyzed with the “Measure” tool of ImageJ. All interval lengths between the labels, and the straight end-to-end distances of the detected chains were determined. In activated cells only chains found outside ORAI1-accumulations were measured.

For the analysis of ORAI1 distribution in punctae all recorded images from all maximally SOCE-activated cells were visually inspected in order to identify images displaying punctae. These punctae were defined as regions of locally accumulated labeled ORAI1 with at least 2-times higher label densities than in the surrounding regions, limited by a visually identifiable border towards the surrounding regions of lower ORAI1 density. Accumulated ORAI1 areas of strand- or ring-like shapes were excluded from the analysis, due to the difficulty of defining their borders. Images containing punctae covered 58% of the total number of images of plasma membrane areas from the group of maximally SOCE activated cells. Punctae areas were manually marked in the images as regions of interest (ROI) using the “Freehand selection” tool in ImageJ, and their area size was determined with the “Measure” tool. Thereafter, the labels inside the ROIs were blanked, by filling the ROIs with background color, and the remaining number of labels in the regions outside the ROIs was again determined using the “Find particles” tool, similarly as done previously for all recorded

images (as explained in the previous paragraph). The difference between the number of particles detected outside the ROI and the total number of particles in the respective image yielded the number of particles within the ROI.

Statistical analyses

Statistical significance for Fig. S3 was performed using paired Student's *t*-test. Differences were considered significant at $p < 0.05$ and are indicated in the Fig.s as follows: $*p < 0.05$, $** p < 0.01$ and $*** p < 0.001$. Cluster analysis for Fig. S4 was performed using software of local design programmed in Java for Image J. Automated line searching was performed in software of local design programmed in c++.

RESULTS

Preparation of cells with labeled ORAI1

For the examination of the two-dimensional plasma membrane distribution of ORAI1 using LPEM, a HEK cell line was used pre-selected for a low background level of endogenous ORAI1. Details on this cell line, named CRI1, are described elsewhere (12).. For experiments with ORAI1 at rest, the cells were transfected with HA-tagged ORAI1. Cells were grown on microchips, as needed for LPEM (24), and chemically fixed prior to ORAI1 labeling with QD nanoparticle labels (13). Fig. 1b displays a typical light microscopy (LM) image from these cells in which several cells expressed ORAI1, which is visible from the fluorescence of green fluorescent protein (GFP) co-expressed in a 1:1 molar ratio. The GFP expressing cells also bind the QD labels thus verifying the specificity of the HA-ORAI1 tag (Fig. 1c). Under resting conditions, ORAI1 remained mostly homogenously distributed throughout the plasma membrane.

To study the effect of SOCE-activation, the same cell line was used but here ORAI1-HA was co-expressed with STIM1 in a 1:3 ratio, and the cells were incubated for 15 min with 1 μM Tg at 37 °C for activation. The 1:3 ratio is known to be optimal for activation of the ORAI channels (25), and was achieved by transfected the expressing plasmids in this ratio (26). To examine the effects of a suboptimal STIM1:ORAI1 ratio, a third experimental group was also prepared in which ORAI1 and STIM1 were expressed in a 1:1 ratio, thus achieving a sub-maximal SOCE-activation after Tg incubation.

Control experiments were performed with another HEK cell line, lacking both endogenous STIM1 and STIM2 (14) to exclude that endogenous, pre-activated STIM1 or STIM2 had an influence on the distribution of ORAI1 (27) (see Fig. S1). A second series of control experiments were performed to examine possible influence of (residual) endogenous levels of ORAI1-3 proteins on the observed ORAI1 spatial distribution by expression in a triple ORAI1-3 knock-out cell line (see Fig. S2). Thirdly, to ensure that the observed effects after SOCE activation were not specific to or an artifact of Tg incubation, incubation with cyclopiazonic acid (CPA) was tested as well, as alternative SOCE activator (see Fig. S3).

LPEM revealed ORAI1 clusters with supra-molecular dimensions

LPEM experiments of whole cells were carried out to map the positions of individual ORAI1 proteins. Using the QD fluorescence intensities of the LM images (Fig. 1c), cells were selected for analysis with STEM. In each experiment, cells from three groups were selected, exhibiting low-, medium, or high ORAI1 expression. Note that the average expression level differed between experiments, and, therefore, the relative expression levels in an experiment were used to define the three groups. STEM images revealing the positions of QD-labeled ORAI1 proteins were thus recorded from dozens of cells, yielding several hundred thousand of single ORAI1 positions (see Table 1). Fig. 2a depicts the typical ORAI1 distribution in a

resting cell; shown is the original STEM image with an overlay of automatically detected QD labels.

It appeared by eye that the ORAI1 distribution was not random, but showed clustering in groups of less than ten labels. To enhance the visibility of ORAI distribution patterns, QD-positions were marked by dots of 17 nm diameter (representing the overall QD size including organic coating). Examples of the observed small clusters are shown in Fig. 2b-e. A possible origin of these small clusters is the attachment of multiple QDs to ORAI1 tetramers or hexamers forming a channel, which would result in a cluster of a diameter of ~40 nm (see Fig. 1a). However, most clusters were larger than 40 nm, and can thus not have originated from single ORAI1 channels but must have originated from clustered channels. It can be reasonably assumed that the clusters larger than 40 nm did not originate from labeled ORAI1 channels that disassembled after labeling, because the proteins were chemically fixed. Moreover, a number of clusters contained more than 6 labels. Many of these clusters had an elongated shape, or formed chains up to 150 nm length (see examples in Fig. 2b-e). To characterize the dimensions of these chain-like protein arrangements, they were examined for their label intervals, and for their overall lengths. These measurements revealed an average label-label distance of 22 ±6 nm (Fig. 2f) with a chain length of 80 ±21 nm (Fig. 2g) for resting cells. In the typical STEM image of Fig. 2a the fraction of ORAI1 in clusters consisting of 4 or more labels was 6-times higher compared to a simulation of randomly positioned labels at the same surface density (see Fig. S4). In addition, linear chains of ≥4 labels with the typical dimensions shown in Fig. 2f and g found in the ORAI1 distribution, and these appeared with a factor of 5 higher probability than for randomly positioned labels at the same surface density (Fig. S4). It can thus be concluded that the supra-molecularly sized ORAI1 clusters were formed by a biological interaction occurring at the plasma membrane. Note that these ORAI1 clusters were not an artifact of highly overexpressed ORAI1, because

they were also found on cells with lower than average expression levels (see Fig. S5). These supra-molecular complexes are also found in cells lacking endogenous STIM (Fig. S2) and in triple ORAI knock-out cells (Fig. S2), thus excluding complexes formed by endogenous STIM or ORAI proteins.

SOCE activation partially relocates ORAI1 into distinct accumulation areas

After maximal SOCE-activation, typical bright ORAI1 punctae were seen in the LM images (Fig. 3a). LPEM revealed that ORAI1 accumulated in oval areas, presumably the ER plasma membrane contact zones, as shown in the STEM image in Fig. 3b. ORAI1 distributions in the punctae were crowded, but it was still possible to regionally recognize chain-like arrangements, suggesting that the dense ORAI1 accumulation areas also included supra-molecular ORAI1 clusters (Fig. 3c). Outside the punctae, a similar spatial distribution of ORAI1 was found as in the resting cells containing small clusters of labels including chain-like ORAI1 arrangements (Fig. 3b and d). The average distance of 22 ±6 nm between labels was equal to the measured value in resting cells (Fig. 2f), a similar match was found for the chain length amounting to 84 ±27 nm in activated cells (Fig. 2g). Occasionally, STEM images revealed much longer chains as described below. The activation-induced ORAI1 accumulations in punctae had diameters of 1.3 ± 0.5 μm for the long axis, 0.7 ± 0.2 μm for the short axis, an aspect ratio of 2.0 ± 0.6, and the average covered area amounted to 0.9 ± 0.5 μm^2 as directly measured from STEM images (Fig. 3e). These values confirmed the dimensions of ER plasma membrane contact zones determined with photoactivated localization microscopy (PALM) from a fluorescent, junctional marker protein (28). Similar ORAI1 punctae were also found after SOCE-activation with CPA, although with smaller dimensions (see Fig. S3).

We wondered if the accumulations of ORAI1 were obtained by additional protein insertion from intracellular stores into the regions of punctae (11) or rather via relocation of

ORAI1 from the surrounding plasma membrane. Insertion of additional protein does not seem likely since the average surface density of ORAI1 was similar between resting- and activated cells (see Table 1). Furthermore, whereas the average density of labels inside regions of punctae had increased by 450%, from 155/μm^2 at rest to 694/μm^2 inside the punctae, the average label density outside punctae had dropped by 10% to 139/μm^2. Although the area occupied by punctae amounted only to 4% of the total imaged area in all analyzed plasma membrane regions of maximally activated cells, these regions contained 18% of all detected labels, revealing that 13% of the total ORAI1 proteins had redistributed into the regions of punctae.

ORAI1 patterns under limiting STIM conditions

After sub-maximal SOCE-activation due to insufficient STIM1 abundance, by using a 1:1 co-expression ratio with ORAI1, a somewhat different clustering pattern of ORAI1 emerged compared to the maximal SOCE activation. Accumulated ORAI1 appeared in larger, irregularly shaped, and more diffuse patches (Fig. 4a). In the STEM images, the borders of ORAI1 accumulation areas emerged less defined than in maximally activated cells (Fig. 4b and d), and the label crowding was less dense (Fig. 4c and e). As for the resting cells and the maximally activated cells, supra-molecular ORAI1 clusters in the sub-maximally activated cells were found outside and inside the accumulation areas. Sometimes, only small groups of two or three chain-like ORAI1 clusters had aligned in a parallel manner (Fig. 4e) (additional examples of STEM images from sub-maximally activated cells are shown in Fig. S6). These results support the idea that dimers of activated STIM1 proteins crosslink neighboring ORAI channel complexes upon activation (14).

Punctae are not the only type of structures in activated cells

Besides the typical ellipsoid ORAI1 punctae found after SOCE-activation several other two-dimensional (2D) structures were found as well in the plasma membrane. Fig. 5a shows examples of micron-long, parallel running ORAI1 formations (indicated with transparent red lines). These ORAI1 strand-like patterns meandered in regions corresponding to areas with a brighter background than the surrounding. Since the contrast in STEM increases with mass, the white shapes represent thickened cellular regions. In addition, four oval ORAI1 punctae were present (outlined with dashed lines). Fig. 5b, recorded from a cell with a low ORAI1 expression, also showed several micron-long strands running in parallel, thus ruling out that these 2D-structures were an artifact of highly overexpressed ORAI1. Such ORAI1 strands were found in 27% of the recorded STEM images from maximally SOCE-activated cells. Fig. 5c, shows examples of ORAI1 punctae differing from the typical ones by their ring-like structures; the largest ring-structure had densely accumulated strands of ORAI1 in its center. These peculiar 2D-structures must have been created by an underlying mechanism elicited by SOCE-activation, and were also found in experiments using CPA induction of SOCE-activation (see Fig. S3).

DISCUSSION

Our study aimed to elucidate how the spatial organization of ORAI1 proteins in the plasma membrane changes upon Ca^{2+} channel activation. We have used an HA-tagged ORAI1 protein in combination with a two-step QD labeling approach, resulting in a label:target ratio of <1, thereby excluding any artificial clustering effect of the labels (12). The proteins were detected in the intact and hydrated cell, using correlative light microscopy and LPEM, yielding the position information of several hundred thousand of single-labeled ORAI1 proteins; this method has a spatial resolution of ~2 nm (20).

In resting cells, we discovered that ORAI1 often assembled in chain-like structures extending up to 150 nm, ORAI1 proteins thus generally tend to form supra-molecular arrangements, consisting of at least 2 and up to probably 4 connected channels. The existence of these ORAI1 conformations contradicts the assumption that ORAI1 channels predominantly exist as independent, freely moving entities, randomly distributed in the plasma membrane (26, 29). Upon SOCE-activation, the ORAI1 clusters appear to have been trapped and dragged into the punctae containing densely agglomerated ORAI1. Measurements of ORAI1 densities inside versus outside punctae revealed on average a 4.5-fold increase, achieved by the redistribution of ~13% of all plasma membrane-bound ORAI1. Our results do not support earlier findings reporting the insertion of ORAI1 from intracellular pools into punctae after SOCE-activation (11). Such a replenishment of plasma membrane localized ORAI1 would increase the average ORAI1 surface density in SOCE-activated cells versus cells at rest, however the average ORAI1 densities in our experiments remained very similar. A possible reason for this discrepancy might be the exclusive use of formaldehyde as fixation agent in the earlier study, which is known to insufficiently fix membrane proteins (30, 31) and to induce artificial redistributions of ORAI1 proteins (32).

Another study by Perni et al. (29) used the method of freeze-fracture electron microscopy to examine overexpressed, unlabeled ORAI1, and found micron-sized patches with ragged edges in the plasma membrane for cells at rest, assuming these areas contained dense accumulations of ORAI1 channels. The authors further suggested that single channels were freely moving within these patches. On the contrary, results obtained by measuring ORAI1's diffusion coefficient in living cells indicated that most ORAI1 proteins were not freely diffusing, which could be explained by the existence of differently sized molecular assemblies (2, 33), a finding which fits to the variability of ORAI1 cluster sizes found in the STEM images. The freeze-fracture method did confirm the presence of puncta, but the

observations did not include strand-like 2D structures after Tg-activation, possibly due to the difficulty of discerning such patterns amongst the other neighboring proteins in the crowded environment of the plasma membrane without using labels.

A possible function of clustering of ORAI1 in supramolecular arrangements could be a more efficient concentration process of ORAI1 Ca^{2+} channels in punctae upon SOCE activation compared to a mechanism via the collection of single channels. The capturing and dragging of only one ORAI1 protein belonging to a supramolecular cluster will drag all the others with it, until the whole cluster reaches the ER plasma membrane contact zone. A confluent filling of the plasma membrane areas located above the accumulated STIM in the ER plasma membrane contact zones, by supra-molecular ORAI1 clusters, instead of single ORAI1 channels, would not only be faster, but would also help in achieving a more homogenous filling, avoiding a jamming of ORAI1 channels at the periphery of the punctae, which would hinder and delay the filling of the more central areas. An amplifying effect, due to the import of supra-molecular ORAI clusters instead of single ORAI1 channels, would lower the required amount of effectively trapped and transported ORAI1 far below the 13% of ORAI1 proteins found to be redistributed after maximal SOCE-activation. Such an amplifying effect would, for instance, play an important role in the immune system, by accelerating the formation of immune synapses between T cells and antigen-presenting cells (34).

The comparison of ORAI1 distributions in accumulation zones in sub-maximally activated cells revealed less dense accumulations of ORAI1 clusters than in maximally activated cells. Yet, some of the accumulation areas showed aligned supra-molecular ORAI1 clusters, further supporting the concept that the import of supra-molecular ORAI1 clusters contributed to the accumulation of ORAI1 in punctae.

The existence of supra-molecular protein clusters in the plasma membrane, with similar dimensions and numbers of involved proteins as detected in this study for ORAI1 is

possibly a general organization principle in the plasma membrane, and was found for other membrane proteins as well, mainly by using super-resolution fluorescence microscopy. After over-expression in HEK cells, for instance, about half of the NMDA receptors were found in clusters containing up to 12 receptors (35). Also, for the family of G-protein coupled receptors, about half of the μ-opioid receptors, and 85% of κ-opioid receptors were reported to reside in clusters with dimensions of 80 – 100 nm, comprising on average 8 and 9 receptors, respectively (36).

It is not known if a linking protein, responsible for the organization of supra-molecular ORAI1 clusters, exists. STIM proteins fulfill such an ORAI1 binding function and concomitant to binding, activate ORAI1 channels in the punctae. But, outside these regions and at rest, clustering of ORAI1 due to STIM is excluded, as was confirmed by control experiments (see Fig. S1).

In conclusion, we found that most ORAI1 channels were organized in small clusters of supra-molecular size ranging from 50 – 150 nm, often arranged into a chain. After SOCE-activation, 13% of plasma membrane-bound ORAI1 reorganized into regions (punctae) of high surface density of oval shape. In addition, a variety of other 2D structures appeared, most of them micron-long strands, and also ring-like patterns. We propose that the supra-molecular ORAI clusters serve an amplifying function for SOCE-activation, by reducing the required number of directly trapped ORAI1 proteins for subsequent accumulation in punctae, as needed for efficient activation by STIM1 proteins in order to induce Ca^{2+} influx.

SUPPORTING MATERIAL

Supporting Material can be found online at

AUTHOR CONTRIBUTIONS

D.B.P, B.A.N, and N.J designed research; D.A. provided ORAI constructs and cells; D.B.P. performed experiments, and analyzed data; D.B.P., B.A.N. and N.J. wrote the paper.

ACKNOWLEDGEMENTS

We thank Sercan Keskin, and Peter Kunnas for help with the STEM, Don Gill for the kind gift of HEK_STIM cells, Daniel Gaa for writing ImageJ plugins, and E. Arzt for his support through INM. The research was funded by the DFG SFB1027 (project C7).

REFERENCES

1. Dynes, J. L., A. Amcheslavsky, and M. D. Cahalan. 2016. Genetically targeted single-channel optical recording reveals multiple Orai1 gating states and oscillations in calcium influx. Proc. Natl. Acad. Sci. 113:440-445.
2. Wu, M. M., E. D. Covington, and R. S. Lewis. 2014. Single-molecule analysis of diffusion and trapping of STIM1 and Orai1 at endoplasmic reticulum–plasma membrane junctions. Mol. Biol. Cell 25:3672-3685.
3. Madl, J., J. Weghuber, R. Fritsch, I. Derler, M. Fahrner, I. Frischauf, B. Lackner, C. Romanin, and G. J. Schutz. 2010. Resting State Orai1 Diffuses as Homotetramer in the Plasma Membrane of Live Mammalian Cells. J. Biol. Chem. 285:41135-41142.
4. Maruyama, Y., T. Ogura, K. Mio, K. Kato, T. Kaneko, S. Kiyonaka, Y. Mori, and C. Sato. 2009. Tetrameric Orai1 Is a Teardrop-shaped Molecule with a Long, Tapered Cytoplasmic Domain. J. Biol. Chem. 284:13676-13685.
5. Penna, A., A. Demuro, A. V. Yeromin, S. Y. L. Zhang, O. Safrina, I. Parker, and M. D. Cahalan. 2008. The CRAC channel consists of a tetramer formed by Stim-induced dimerization of Orai dimers. Nature 456:116-U112.

6. Mignen, O., J. L. Thompson, and T. J. Shuttleworth. 2008. Orai1 subunit stoichiometry of the mammalian CRAC channel pore. J. Physiol. 586:419-425.

7. Hou, X., L. Pedi, M. M. Diver, and S. B. Long. 2012. Crystal Structure of the Calcium Release–Activated Calcium Channel Orai. Science 338:1308.

8. Cai, X., Y. Zhou, R. M. Nwokonko, N. A. Loktionova, X. Wang, P. Xin, M. Trebak, Y. Wang, and D. L. Gill. 2016. The Orai1 Store-operated Calcium Channel Functions as a Hexamer. J Biol Chem 291:25764-25775.

9. Liou, J., M. L. Kim, W. D. Heo, J. T. Jones, J. W. Myers, J. E. Ferrell, and T. Meyer. 2005. STIM is a Ca2+ sensor essential for Ca2+-store-depletion-triggered Ca2+ influx. Curr. Biol. 15:1235-1241.

10. Mercer, J. C., W. I. DeHaven, J. T. Smyth, B. Wedel, R. R. Boyles, G. S. Bird, and J. W. Putney. 2006. Large store-operated calcium selective currents due to co-expression of Orai1 or Orai2 with the intracellular calcium sensor, Stim1. J. Biol. Chem. 281:24979-24990.

11. Hodeify, R., S. Selvaraj, J. Wen, A. Arredouani, S. Hubrack, M. Dib, S. N. Al-Thani, T. McGraw, and K. Machaca. 2015. A STIM1-dependent ‘trafficking trap’mechanism regulates Orai1 plasma membrane residence and Ca2+ influx levels. J. Cell Sci. 128:3143-3154.

12. Alansary, D., D. B. Peckys, B. A. Niemeyer, and N. de Jonge. 2020. Detecting single ORAI1 proteins within the plasma membrane reveals higher order channel complexes. J. Cell Sci. 133.

13. Peckys, D. B., D. Alansary, B. A. Niemeyer, and N. de Jonge. 2016. Visualizing Quantum Dot Labeled ORAI1 Proteins in Intact Cells Via Correlative Light and Electron Microscopy. Microsc. Microanal. 22:902-912.

14. Zhou, Y., R. M. Nwokonko, X. Cai, N. A. Loktionova, R. Abdulqadir, P. Xin, B. A. Niemeyer, Y. Wang, M. Trebak, and D. L. Gill. 2018. Cross-linking of Orai1 channels by STIM proteins. Proc Natl Acad Sci U S A 115:E3398-e3407.

15. Gwack, Y., S. Srikanth, S. Feske, F. Cruz-Guilloty, M. Oh-hora, D. S. Neems, P. G. Hogan, and A. Rao. 2007. Biochemical and functional characterization of Orai proteins. J Biol Chem 282:16232-16243.

16. Kim, J. H., S.-R. Lee, L.-H. Li, H.-J. Park, J.-H. Park, K. Y. Lee, M.-K. Kim, B. A. Shin, and S.-Y. Choi. 2011. High Cleavage Efficiency of a 2A Peptide Derived from Porcine Teschovirus-1 in Human Cell Lines, Zebrafish and Mice. PLOS ONE 6:e18556.

17. Peckys, D. B., and N. de Jonge. 2015. Studying the stoichiometry of epidermal growth factor receptor in intact cells using correlative microscopy. J. Vis. Exp. 103:e53186.

18. Kusumi, A., and K. Suzuki. 2005. Toward understanding the dynamics of membrane-raft-based molecular interactions. Biochim. Biophys. Acta 1746:234-251.

19. Tanaka, K. A. K., K. G. N. Suzuki, Y. M. Shirai, S. T. Shibutani, M. S. H. Miyahara, H. Tsuboi, M. Yahara, A. Yoshimura, S. Mayor, T. K. Fujiwara, and A. Kusumi. 2010. Membrane molecules mobile even after chemical fixation. Nat. Methods 7:865-866.

20. Dahmke, I. N., A. Verch, J. Hermannsdorfer, D. B. Peckys, R. S. Weatherup, S. Hofmann, and N. de Jonge. 2017. Graphene Liquid Enclosure for Single-Molecule Analysis of Membrane Proteins in Whole Cells Using Electron Microscopy. ACS Nano 11:11108-11117.

21. Textor, M., and N. de Jonge. 2018. Strategies for Preparing Graphene Liquid Cells for Transmission Electron Microscopy. Nano Lett.

22. Hermannsdörfer, J., V. Tinnemann, D. B. Peckys, and N. de Jonge. 2016. The effect of electron beam irradiation in environmental scanning transmission electron microscopy of whole cells in liquid. Microsc. Microanal. 20:656-665.

23. Peckys, D. B., U. Korf, and N. de Jonge. 2015. Local variations of HER2 dimerization in breast cancer cells discovered by correlative fluorescence and liquid electron microscopy. Sci. Adv. 1:e1500165.

24. Peckys, D. B., and N. de Jonge. 2014. Liquid scanning transmission electron microscopy: imaging protein complexes in their native environment in whole eukaryotic cells. Microsc. Microanal. 20:346-365.

25. Scrimgeour, N., T. Litjens, L. Ma, G. J. Barritt, and G. Y. Rychkov. 2009. Properties of Orai1 mediated store-operated current depend on the expression levels of STIM1 and Orai1 proteins. J. Physiol. 587:2903-2918.

26. Hoover, P. J., and R. S. Lewis. 2011. Stoichiometric requirements for trapping and gating of Ca2+ release-activated Ca2+ (CRAC) channels by stromal interaction molecule 1 (STIM1). Proc. Natl. Acad. Sci. 108:13299-13304.

27. Brandman, O., J. Liou, W. S. Park, and T. Meyer. 2007. STIM2 Is a Feedback Regulator that Stabilizes Basal Cytosolic and Endoplasmic Reticulum Ca2+ Levels. Cell 131:1327-1339.

28. Hsieh, T.-S., Y.-J. Chen, C.-L. Chang, W.-R. Lee, and J. Liou. 2017. Cortical actin contributes to spatial organization of ER–PM junctions. Mol. Biol. Cell 28:3171-3180.

29. Perni, S., J. L. Dynes, A. V. Yeromin, M. D. Cahalan, and C. Franzini-Armstrong. 2015. Nanoscale patterning of STIM1 and Orai1 during store-operated Ca2+ entry. Proc. Natl. Acad. Sci. 112:E5533-E5542.

30. Kusumi, A., and K. Suzuki. 2005. Toward understanding the dynamics of membrane-raft-based molecular interactions. Biochimica et Biophysica Acta (BBA) - Mol. Cell Res. 1746:234-251.

31. Huebinger, J., J. Spindler, K. J. Holl, and B. Koos. 2018. Quantification of protein mobility and associated reshuffling of cytoplasm during chemical fixation. Sci. Rep. 8:17756.

32. Demuro, A., A. Penna, O. Safrina, A. V. Yeromin, A. Amcheslavsky, M. D. Cahalan, and I. Parker. 2011. Subunit stoichiometry of human Orai1 and Orai3 channels in closed and open states. Proc. Natl. Acad. Sci. 108:17832-17837.

33. Katz, Z. B., C. Zhang, A. Quintana, B. F. Lillemeier, and P. G. Hogan. 2019. Septins organize endoplasmic reticulum-plasma membrane junctions for STIM1-ORAI1 calcium signalling. Sci. Rep. 9:10839.

34. Hartzell, C. A., K. I. Jankowska, J. K. Burkhardt, and R. S. Lewis. 2016. Calcium influx through CRAC channels controls actin organization and dynamics at the immune synapse. eLife 5:e14850.

35. Yadav, R., and H. P. Lu. 2018. Revealing dynamically-organized receptor ion channel clusters in live cells by a correlated electric recording and super-resolution single-molecule imaging approach. Phys. Chem. Chem. Phys. 20:8088-8098.

36. Tobin, S. J., D. L. Wakefield, L. Terenius, V. Vukojevic, and T. Jovanovic-Talisman. 2019. Ethanol and Naltrexone Have Distinct Effects on the Lateral Nano-organization of Mu and Kappa Opioid Receptors in the Plasma Membrane. ACS Chem. Neurosci. 10:667-676.

TABLES

TABLE 1 Data of ORAI1 labeling experiments including the experiment type. Conditions are at rest, at sub-maximal, and at maximal activation. Information provided is the number of experiments, the number of examined cells, the number of detected labels, the average label density, and the total analyzed membrane area.

Experimental condition	Number of experiments	Number of cells	Number of labels	Label density /µm^2	Analyzed area [µm^2]
ORAI-HA at rest	2	14	157.729	157	1007
ORAI-HA activated by 15 min Tg (with 1:1 STIM1 co-expression)	3	15	245.118	155	1.584
ORAI-HA activated by 15 min Tg (with 1:3 STIM1 co-expression)	3	21	370.946	162	2.292

TABLE 2 Measurements of linear supra-molecular ORAI1 arrangements for cells at rest and maximally activated cells.

Experimental condition	Number of cells	Number of analyzed images	Number of detected label chains	Number of measured label intervals	label interval [nm]	Chain length [nm]
ORAI-HA at rest	5	6	84	303	22 ±6	80 ±22
ORAI-HA activated by 15 min Tg (with 1:3 STIM1 co-expression)	6	7	72	292	22 ±6	84 ±27

TABLE 3 Measurements of ORAI1 distributions in punctae for maximally store-operated calcium entry (SOCE) activated cells.

Experimental condition	Number of cells	% area occupied by punctae	% labels inside punctae	label density inside punctae /µm^2	label density outside punctae /µm^2
ORAI-HA activated by 15 min Tg (with 1:3 STIM1 co-expression)	21	4	18	694	139

FIGURE CAPTIONS

FIGURE 1 Labeling of ORAI1 proteins in the plasma membrane of HEK cells with quantum dots (QDs). **(a)** Schematic representation of QD-labeling of the ORAI1 Ca^{2+} channel in in the plasma membrane. Labels consisted of a biotinylated Anti-HA Fab that bound to the HA-tags (orange spheres) at the extracellular region of each subunit of the ORAI1-HA channel, shown in hexameric conformation (blue and red). The bound Fab was labeled using streptavidin (green) conjugated, fluorescent QDs with an electron dense core (dark gray), and an electron transparent polymer coating shell (yellow). A fully extended configuration of the labels allows for a maximal label distance of ~40 nm. All protein structures were derived from the Protein Data Base, sizes of QDs were measured elsewhere (12) all structures are drawn to scale. **(b)** Overlay of direct interference contrast light microscopy, and fluorescence microscopy of green fluorescent protein (GFP) co-expressed with the same ratio as ORAI1. **(c)** Fluorescence images of QD-labeled ORAI1 at rest showing overlap with the cells expressing ORAI1 visible from GFP in (b). Scale bars = 50 μm.

FIGURE 2 Scanning transmission electron microscopy (STEM) of ORAI1 distributions in whole cells in liquid state. **(a)** Typical STEM image recorded from a resting cell (electron-dense QD cores outlined in yellow, n = 2.817 labels), revealing randomly scattered ORAI1 clusters. **(b-e)** Close-up images of the areas indicated with b-e in (a). For better visibility of two dimensional (2D) patterns, the background was colored white, and black dots of a diameter of 17 nm were drawn at the center position of each label. Several elongated ORAI1 clusters are visible, indicated by a transparent red line. **(f)** Characterization of detected ORAI1 chains by measuring the intra-chain label intervals in cells at rest (n = 301), and after maximal

store-operated calcium entry (SOCE) activation (n = 292). **(g)** Analyzed chain lengths (resting cells: n = 47, Tg-activated cells: n = 72). Small black crosses indicate maximum outliers. Scale bars in a = 1 μm, in b-e = 200 nm.

FIGURE 3 Analysis of ORAI1 punctae in maximally SOCE-activated cells. **(a)** Fluorescence microscopy image depicting the QD signal. Bright dots indicate accumulations of ORAI1 in punctae. **(b)** STEM image showing an ellipsoid area, densely filled with ORAI1. **(c)** Close-up of ORAI1 distribution in the region at the punctae indicated by the left dotted rectangle in (b). **(d)** Close-up of ORAI1 distribution in the region outside the punctae indicated by the right dotted rectangle in (b). **(e)** Measurements of all entirely displayed ORAI1 punctae (n = 44) in STEM images from maximally activated cells (N = 18) indicating the average values and deviations of the length of the long- and short axis, their aspect ratio, and the area of the punctae. Scale bar in a = 50 μm, in b = 1 μm, and in c-d = 200 nm.

FIGURE 4 Analysis of ORAI1 punctae after sub-maximal activation. **(a)** Fluorescence microscopy image depicting the QD signal. Brighter patches indicate accumulations of ORAI1. **(b)** STEM image showing a broad area with increased ORAI1 density. **(c)** Close-up of ORAI1 distribution in the ORAI1-dense region indicated by the dotted rectangle in (b). **(d)** STEM image of another cell exhibiting a lower expression of ORAI1. Here, a region is visible with increased clustering with respect to the remaining area. **(e)** Close-up of ORAI1 distribution in the ORAI1-dense region indicated by the right dotted rectangle in (d). Scale bars in a = 50 μm, in b and d = 1 μm, and in c and e = 200 nm.

FIGURE 5 ORAI1 distributions in activated cells displayed a variety of 2D structures. **(a)** The original STEM image (with QD labels outlined in yellow) provides an impression of the regional cellular morphology, with thicker areas appearing brighter than thinner ones, showing that a bulging membrane topography often coincided with dense accumulations of ORAI1. Typical, oval-shaped punctae (outlined by dashed lines) and nearby running, several micrometer-long strands of aligned ORAI1 (transparent red traces) can be seen. **(b)** A cell with a lower ORAI1 expression level, showing similarly long strands of parallel running ORAI1 chains. **(c)** Flattened ring-like structures of ORAI1 of different dimensions, the larger one enclosing centrally located regions of accumulated ORAI1. Scale bars = 1 μm.

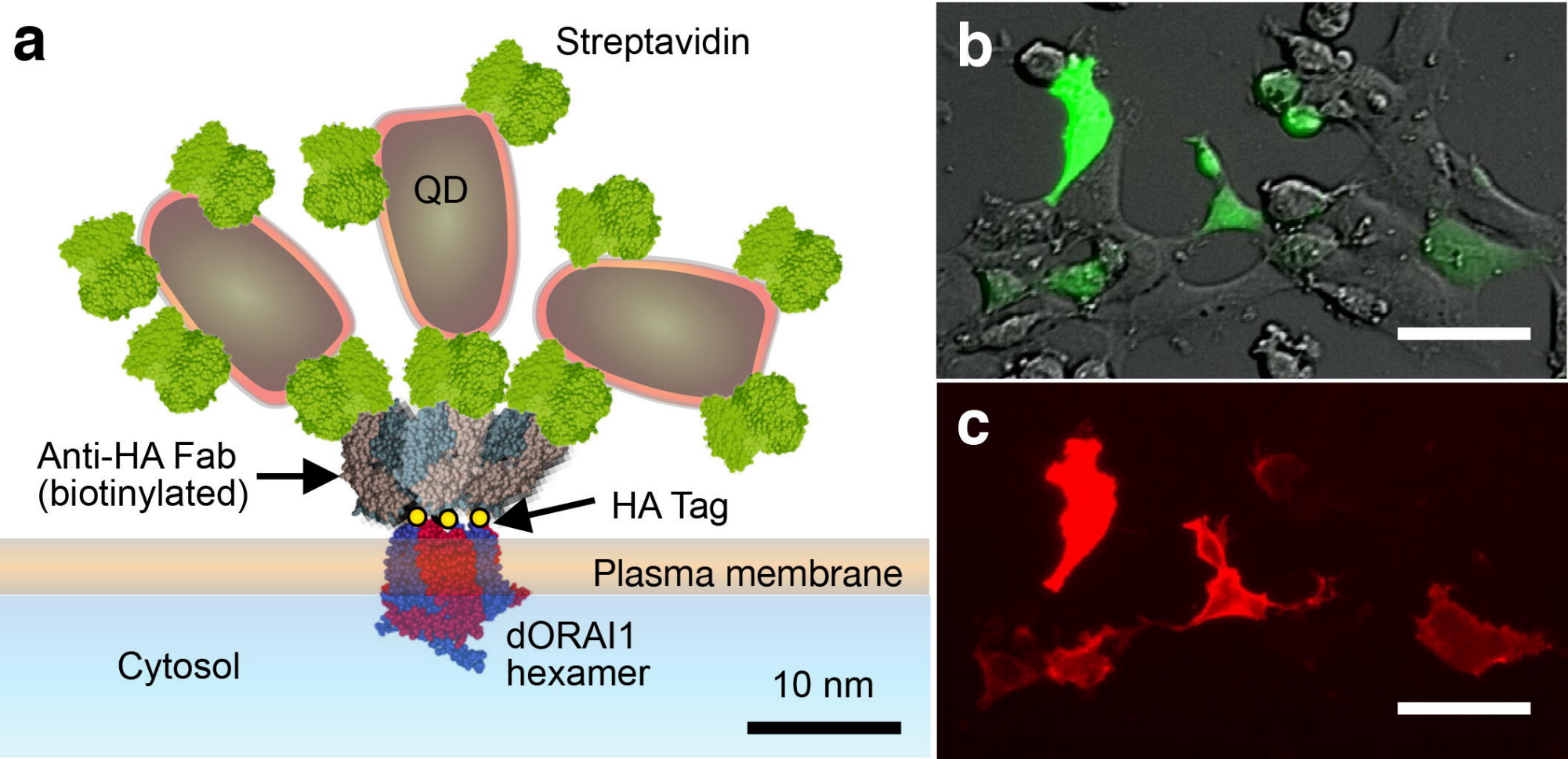
a
Streptavidin
QD
Anti-HA Fab
(biotinylated)
HA Tag
Plasma membrane
Cytosol
dORAI1
hexamer
10 nm
b
c

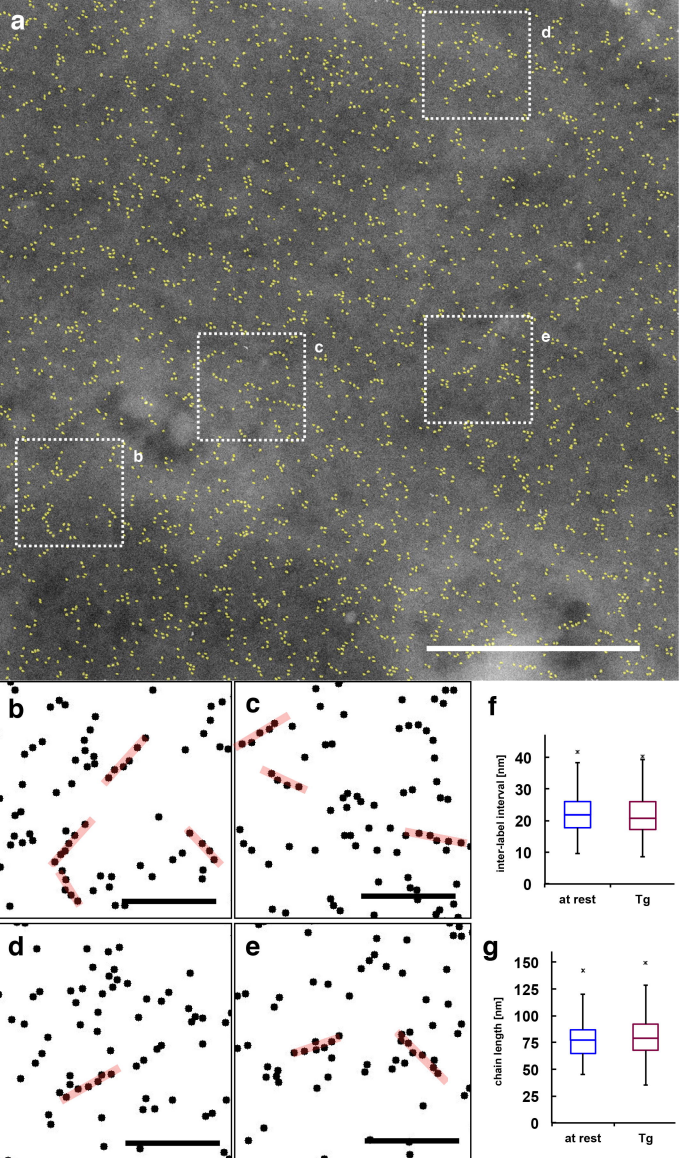
a
b
c
d
e
f
inter-label interval [nm]
40
30
20
10
0
at rest
Tg
g
chain length [nm]
150
125
100
75
50
25
0
at rest
Tg

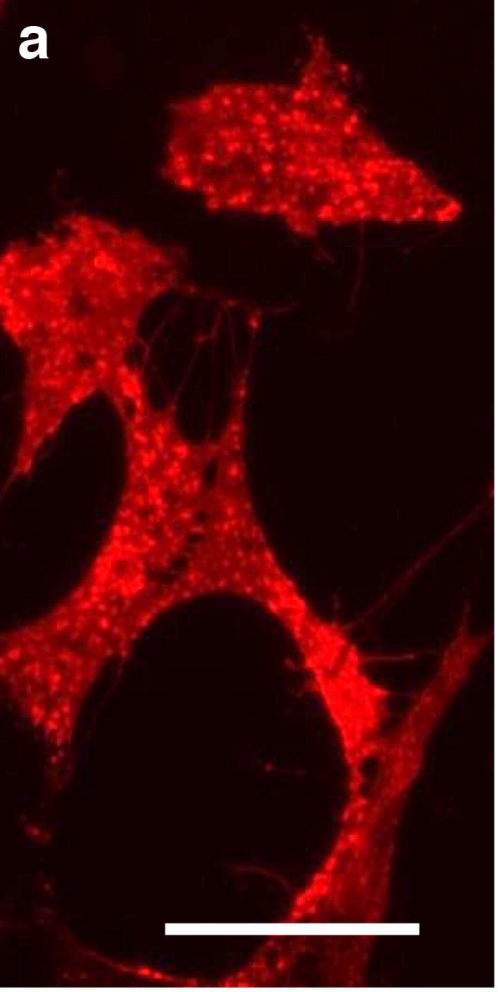
a

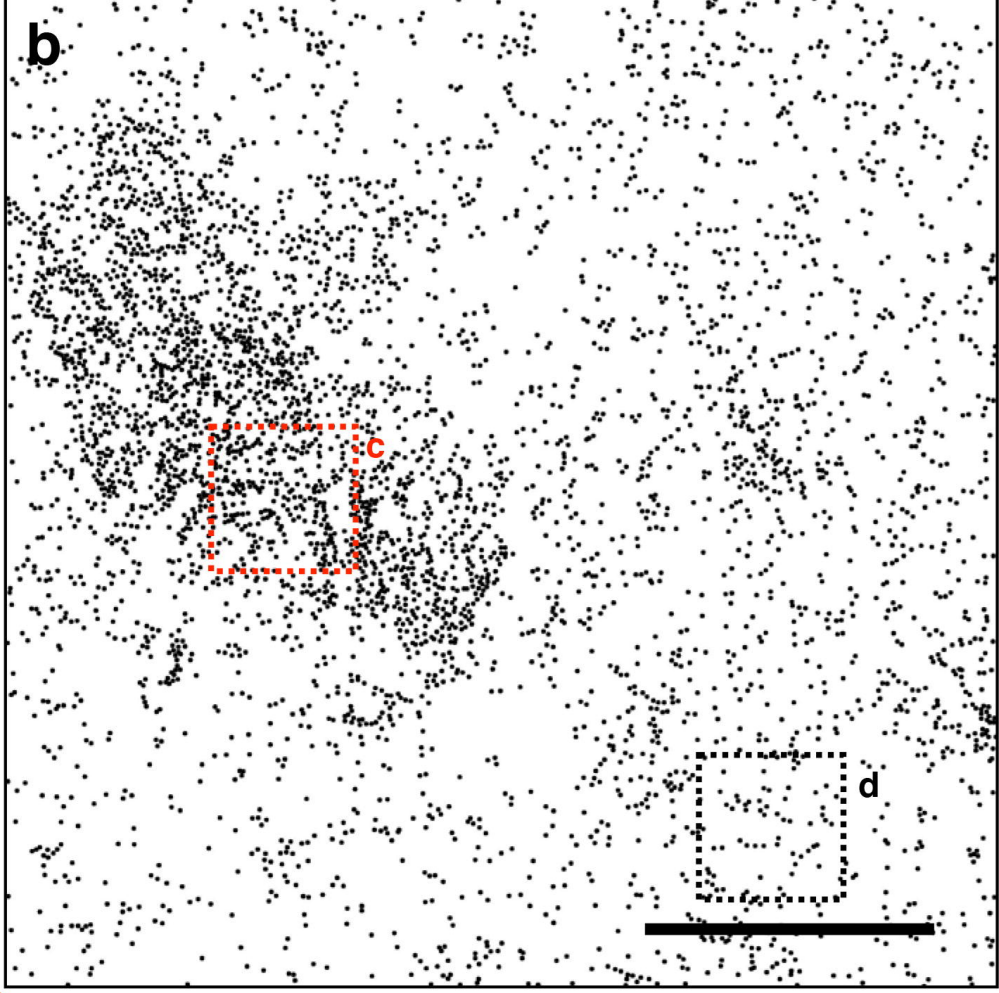
b
c
d

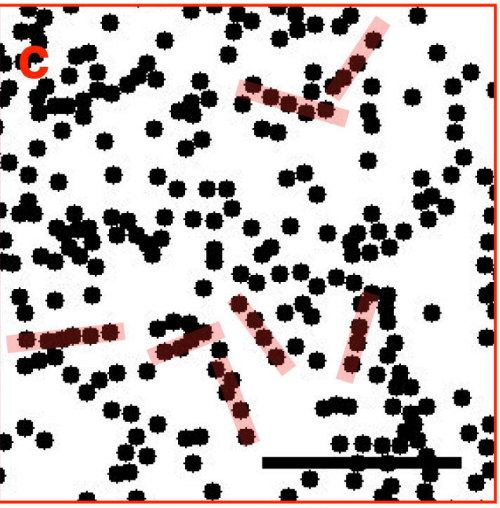
c

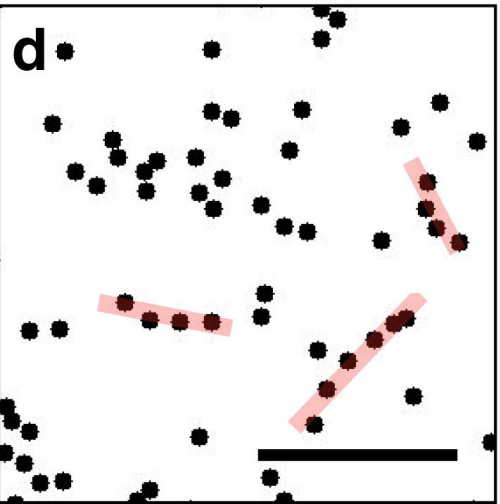
d

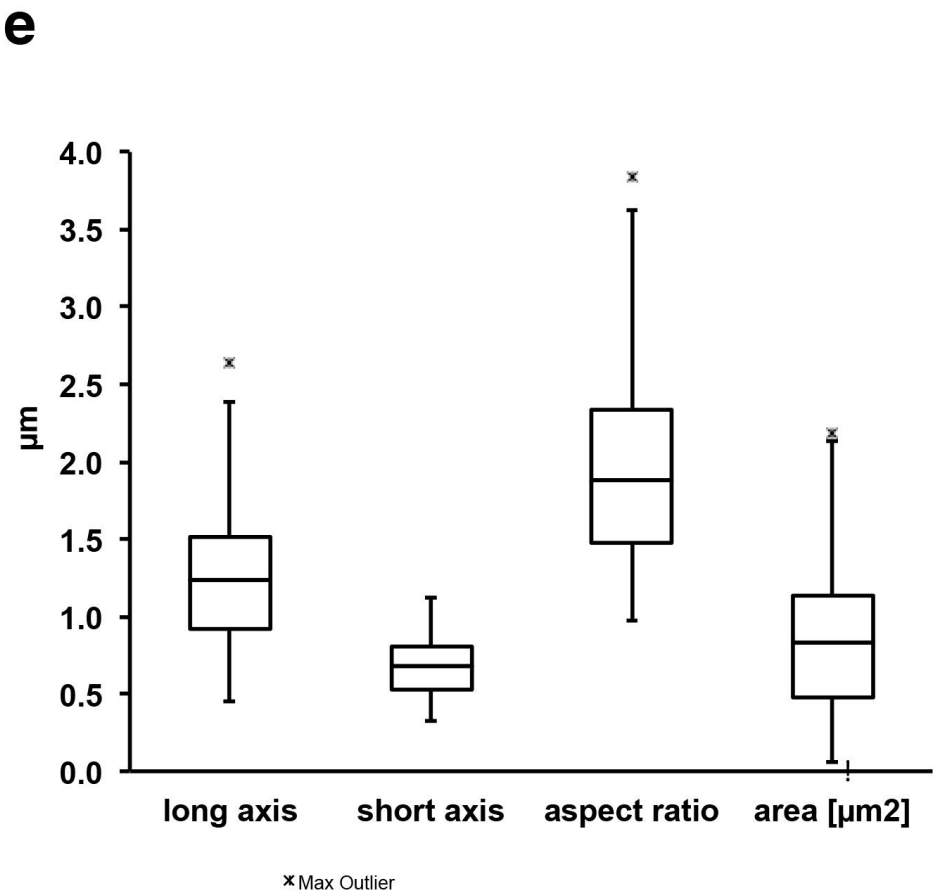
e
µm
4.0
3.5
3.0
2.5
2.0
1.5
1.0
0.5
0.0
long axis
short axis
aspect ratio
area [µm2]
Max Outlier

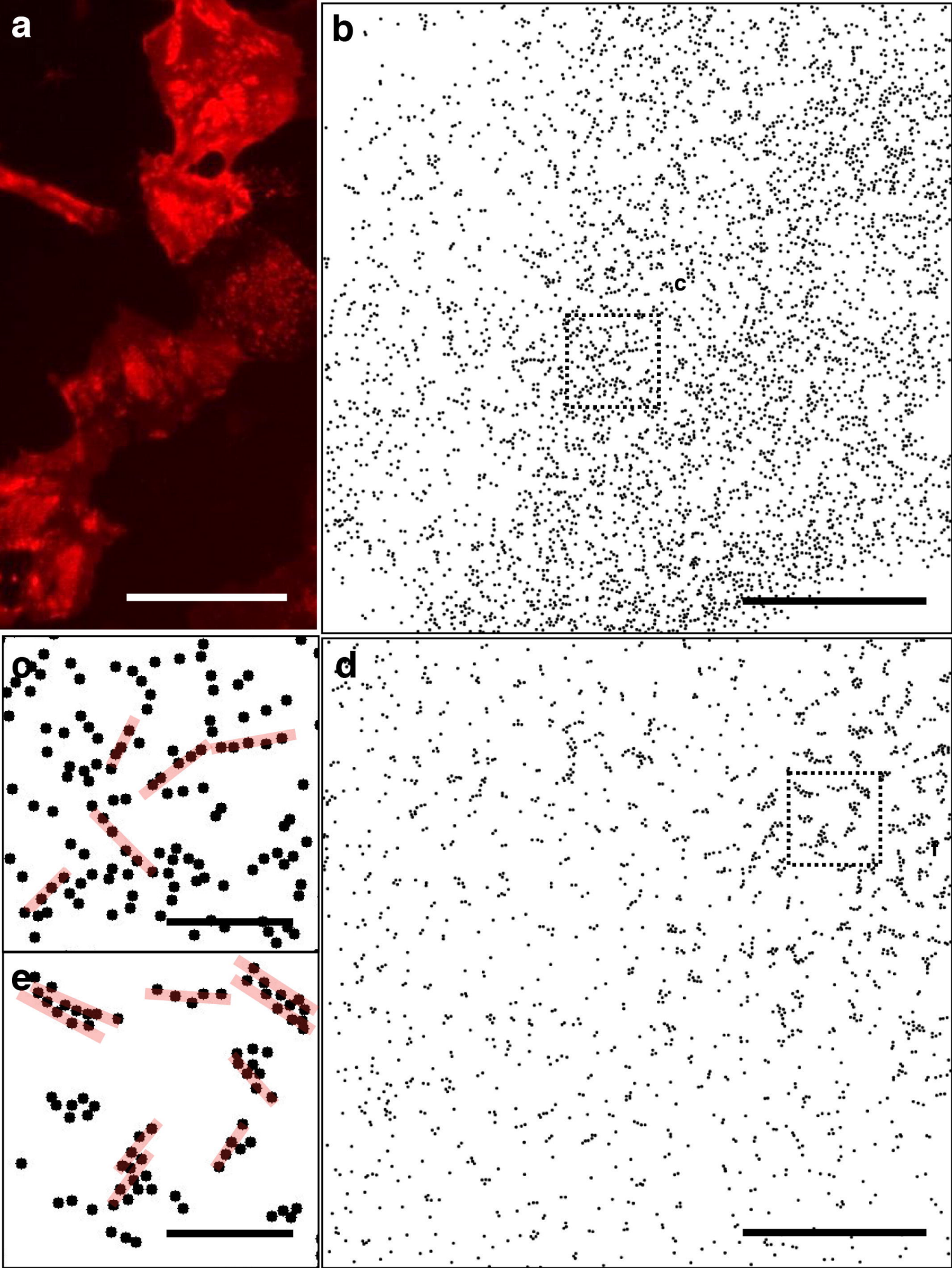
a
b
c
c
d
e

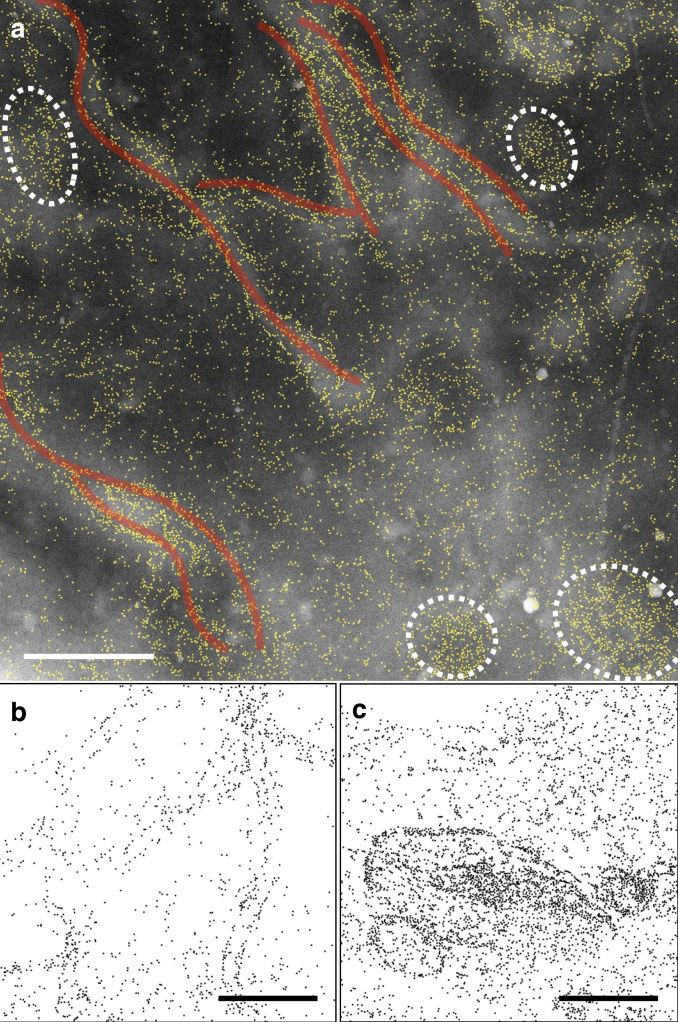
a
b
c